Nanoscale surface electrical properties of indium–tin–oxide films for organic light emitting diodes investigated by conducting atomic force microscopy

Heh-Nan Lin, Sy-Hann Chen, Gung-Yeong Perng, and Show-An Chen

Citation: Journal of Applied Physics **89**, 3976 (2001); doi: 10.1063/1.1353558
View online: http://dx.doi.org/10.1063/1.1353558
View Table of Contents: http://scitation.aip.org/content/aip/journal/jap/89/7?ver=pdfcov
Published by the AIP Publishing

Nanoscale surface electrical properties of indium–tin–oxide films for organic light emitting diodes investigated by conducting atomic force microscopy

Heh-Nan Lin[a)]
Department of Materials Science and Engineering, National Tsing Hua University, Hsinchu 300, Taiwan, Republic of China

Sy-Hann Chen
Department of Electrophysics, National Chiao Tung University, Hsinchu 300, Taiwan, Republic of China and Precision Instrument Development Center, National Science Council, Hsinchu 300, Taiwan, Republic of China

Gung-Yeong Perng and Show-An Chen
Department of Chemical Engineering, National Tsing Hua University, Hsinchu 300, Taiwan, Republic of China

(Received 5 September 2000; accepted for publication 12 January 2001)

Nanoscale surface electrical properties of indium–tin–oxide films prepared by different cleaning methods for use as anode materials in organic light emitting diodes are studied by conducting atomic force microscopy. It is found that most of the surface area possesses a nonconducting feature, and an ultraviolet-ozone treatment produces the most nonconductive sample. The conducting regions, which distribute randomly and range from 6 to 50 nm in size, are attributed to the existence of Sn-rich oxide by a comparison with reported scanning electron microscopy images. After scanning the tip with a bias of −8 V on the nonconducting regions, oxide decomposition occurs on as-received and wet-cleaning processed samples, whereas no structure change appears on the ozone treated sample. The results indicate that the generation of stable oxide after ozone treatment is one of the origins for improved device performance. © *2001 American Institute of Physics.* [DOI: 10.1063/1.1353558]

I. INTRODUCTION

Organic light emitting diodes (OLEDs) have attracted a lot of interest in recent years for their potential to produce low-cost optoelectronic devices.[1,2] Due to its transparency and high electrical conductivity, indium–tin–oxide (ITO) is usually used as the anode material. Typically, ITO is produced by deposition of a mixture of In_2O_3 (~95%–90%) and SnO_2 (~5%–10%), and its high conductivity is due to the oxygen vacancies in In_2O_3 and the extra electrons from the doped Sn atoms.[3] However, it is well known that the surface properties of ITO, such as the roughness, work function (WF), etc., have a significant influence on device performance.[4–6] Furthermore, different ITO cleaning procedures also change these properties and thus the efficiency achieved.[4–6]

Since the organic emissive layer typically has a thickness of around 100 nm or less, it would be advantageous to have an understanding of the nanoscale electrical properties of ITO. Also, experimental results of such kind will shed light on the microscopic origins of the factors affecting device operation. However, such an endeavor has not been realized to our knowledge. In this article, we employ conducting atomic force microscopy (AFM)[7–9] to investigate surface electrical properties of ITO films prepared by different cleaning methods. The results provide evidence that the production of stable oxide on ITO contributes to higher efficiency and better stability.

II. EXPERIMENT

The experiment was performed under ambient conditions using a commercial AFM (Dimension 3100, Digital Instruments). Rectangular Si tips (CSC17, NT-MDT, Russia) with an estimated spring constant of 0.15 N/m were used in contact mode for simultaneous topography and current measurements. The contact force was maintained at around 60 nN as determined from a force–distance plot. The tips were precoated with a Cr layer by the manufacturer and subsequently coated with a 15 nm Au film by ion sputtering. Bias voltage was applied to the tip through electronics in the AFM and the ITO was grounded. The current was amplified by a preamplifier (SR-570, Stanford Research Systems) and sent to the AFM controller through a signal access module. A 1 kΩ resistor was put in series for protection.

Commercially available ITO films (SLR, Sanyo Vacuum Industry, Japan) with a thickness of around 150 nm on glass substrates were used for experiment. Three samples were tested. Sample A was the as-received specimen. Sample B was cleaned in isopropyl alcohol for 30 min, CH_2Cl_2 for 30 min, and H_2O_2/NH_4OH/de-ionized water (1:1:5) solution for 60 min. Sample C was first cleaned by the same steps as sample B, and then treated by ultraviolet (UV)-ozone for 60

a)Electronic mail: hnlin@mse.nthu.edu.tw

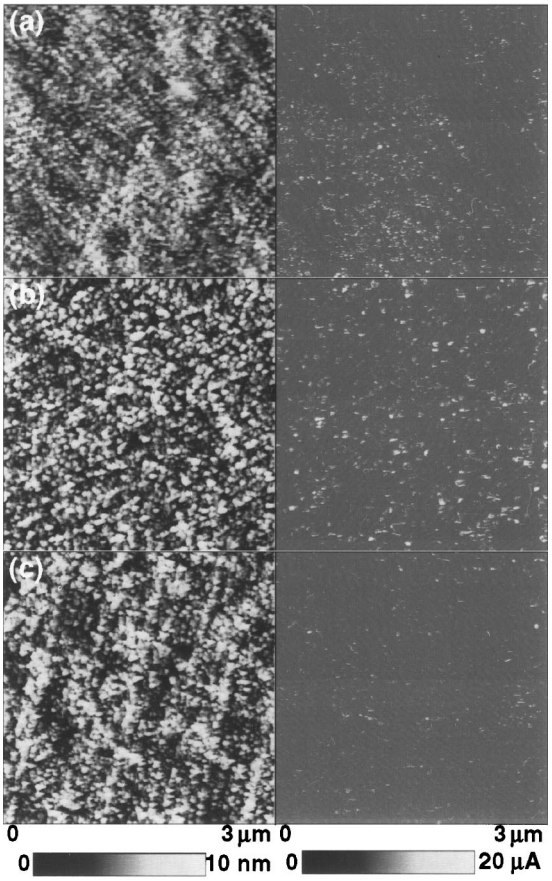

FIG. 1. Topography (left) and current images (right) of (a) the as-received, (b) the wet-cleaning processed, and (c) the wet-cleaning and UV-ozone treated ITOs. The tip was biased to −0.5 V and the ITO was grounded.

min. All the above wet cleaning procedures were performed in an ultrasonic bath.

III. RESULTS

With a bias of −0.5 V applied to the tip during scanning, the topography (left) and current (right) images of the three ITO samples are shown in Fig. 1. Various dot structures ranging from 30 to 90 nm in size are on the surfaces and the root-mean-square roughness values are 1.4, 2.4, and 2.3 nm, respectively. Obviously, the wet cleaning procedure increased the surface roughness, whereas the UV-ozone treatment had little effect.

In the current images, conducting and nonconducting regions both exist on the surfaces with the former signified by bright contrast. Apparently, most of the surface area has a nonconducting feature. On the other hand, conducting regions distribute randomly, with sizes ranging from 6 to 50 nm. The smallest value of 6 nm is confirmed by higher resolution images (not shown) and is in reasonable agreement with the estimated tip–sample contact diameter of 7.4 nm obtained from a simple Hertz contact mechanics calculation.[10] The percentage of coverage of these two regions can be obtained from the current distribution histograms, which are plotted in Fig. 2. If we consider the points below 1 μA nonconducting, 92% of the surface area is nonconducting on samples A and B, and 97% of the surface area

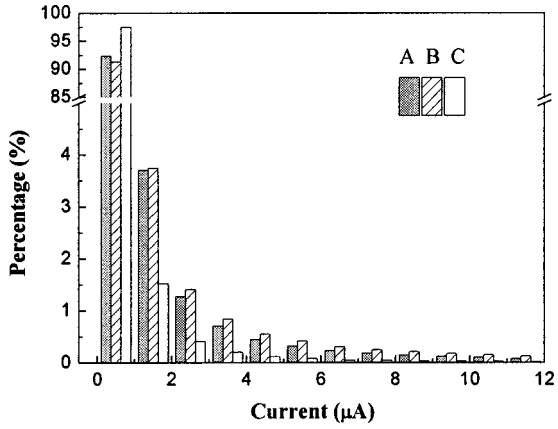

FIG. 2. Histograms of the current distribution for the three current images in Fig. 1.

on sample C is nonconducting. The distributions for samples A and B are quite similar, but sample B is slightly more conductive than sample A.

The identities of the conducting and nonconducting regions on the ITO surface can be explained by a direct comparison with scanning electron microscopy results. From a recent study of the surface structures of homemade (after heat treatment) and commercially available ITO films,[11] In_2O_3, SnO, and Sn-rich oxides ($Sn_{n+1}O_n$ and $Sn_{2n}O_{2n-1}$) are found to be present on the surface, which also indicates the decomposition of SnO_2 in the deposition process. Since Sn-rich oxides have higher conductivities, it is reasonable to correlate the conducting regions in Fig. 1 to Sn-rich oxides and the nonconducting regions to In_2O_3 or SnO. Furthermore, it can be argued that the slightly higher presence of more conducting regions on sample B compared to on sample A was due to the reduction of SnO since H_2O_2 in an alkaline solution facilitates reduction. On the other hand, the UV-ozone treatment assisted oxidation of Sn-rich oxides into SnO and made sample C the most nonconductive (see below).

To further verify the above assessments, we also performed local current–voltage ($I-V$) measurements. A typical $I-V$ relationship on the conducting regions of the three samples is shown in Fig. 3(a). (Note that the current is much higher than that in Fig. 1 at bias of 0.5 V, which is due to the formation of a more stable contact in the $I-V$ measurement.) From the linear behavior, the contact is apparently an ohmic contact. The point contact resistance is calculated to be around 1.2 kΩ after subtracting the 1 kΩ resistance. Two theoretical formalisms can be used to obtain estimates for a comparison. The first is a classical expression for spreading resistance R, which is represented as[7,8]

$$R=\frac{\rho_1+\rho_2}{4a}, \tag{1}$$

where ρ_1 and ρ_2 are the resistivities of the two materials in contact and a the contact radius, which is around 3.7 nm.[10] Since the resistivity of ITO is around $3\times10^{-4}\,\Omega$ cm,[3] which is about two orders of magnitude higher than that of Au, Eq. (1) gives a contact resistance of around 200 Ω. The result is

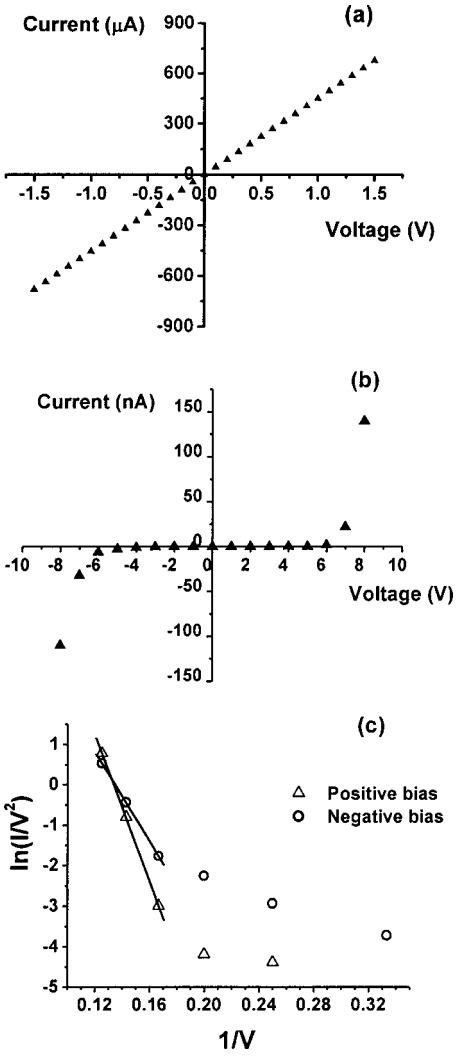

FIG. 3. Typical $I-V$ curves on (a) the conducting regions on the three samples, (b) the nonconducting regions on sample C, and (c) the Fowler–Nordheim plot of the absolute I, V values in (b). Note that $I-V$ measurements on nonconducting regions on samples A and B did not give reproducible results.

much less than the experimental value. However, a criterion for Eq. (1) is that a should be greater than the electron mean free path, which is apparently not fulfilled since the electron mean free path in metals is typically around 10 nm.

A more accurate description of the contact resistance R is Sharvin's formula,[8,9]

$$R=\frac{4\rho\lambda}{3\pi a^2}, \tag{2}$$

where λ is the electron mean free path. Although Eq. (2) holds for nanoscale confinement in a homogeneous material, which is different from our present case, it is still useful for a reasonable estimate. If we use $\lambda=10$ nm, the result is 930 Ω, in good agreement with the experimental result.

A typical $I-V$ curve of the nonconducting regions on sample C is shown in Fig. 3(b). The current increases significantly when the voltage is above 5 V. Apparently, a

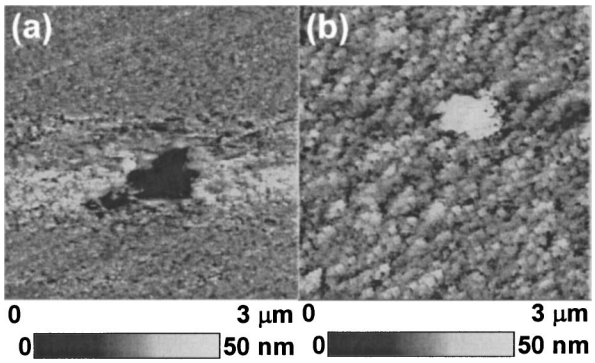

FIG. 4. Topography images of sample B after the application of tip biases of (a) -8 and (b) $+8$ V in a prescanning area of 0.5×0.5 μm^2. The sizes of the crater in (a) and the hillock in (b) are both around 0.6 μm. The depth in (a) and the height in (b) are approximately 30 and 25 nm, respectively.

Fowler–Nordheim type of electron tunneling[6] is responsible for the detected current. In this situation, the $I-V$ relationship can be linearized and expressed by

$$\ln\left(\frac{I}{V^2}\right)\propto-\frac{1}{V}+\text{const.} \tag{3}$$

To verify this, a plot of $\ln(I/V^2)$ vs $1/V$ is shown in Fig. 3(c) and a linear relationship is observed at high voltage as expected. Also from Fig. 3(c), the tunneling current is higher at a negative tip bias except at the bias of 8 V. This can be explained by the $I-V$ behavior of an asymmetric metal–insulator–metal tunnel diode.[12] Since the WFs of ozone-treated ITO and Au are around 4.7 and 5.1 eV, respectively, a higher tunneling current is expected at a large negative tip bias.[12]

$I-V$ measurements of the nonconducting sites on samples A and B, however, gave very different results. At the first voltage ramp, the current also increased significantly when the bias was above 5 V. But at the second ramp, the nonconducting sites became conducting and ohmic contact behavior appeared. Various regions on both samples were tested, but a similar phenomenon was observed. To further explore this phenomenon, a high voltage of -8 or $+8$ V was first applied to the tip in a scanning area of 0.5×0.5 μm^2, and a larger area of 3×3 μm^2 was imaged in the second scanning with the tip bias reduced to -0.5 V. This measurement was performed on samples C and B, and there was no structural change on the former's surface as expected. The results on sample B are shown in Fig. 4, where a crater with a depth of 30 nm and a hillock with a height of 25 nm are present in Figs. 4(a) (-8 V) and 4(b) ($+8$ V), respectively. Both the crater and the hillock have similar diameters of around 0.6 μm. The current images were not reproducible, which was probably caused by peeloff of the Au film, and are not presented. The crater formation should be related to the decomposition of In_2O_3 or SnO due to the high electric field. The hillock formation is possibly related to field evaporation of the tip material,[13] local oxidation,[14] or dielectric

breakdown.[15] Details of the mechanisms for the structural change, however, are beyond the scope of the present work.

IV. DISCUSSION

It has so far been evidenced that stable oxide existed on sample C, but not on samples A and B. As a result, it is reasonable to relate the occurrence to more complete oxidation after the UV-ozone treatment. The results also shed light on issues related to OLED efficiency and stability. It is widely accepted that UV-ozone or oxygen plasma treated ITOs usually give higher efficiencies than as-received or wet-cleaning processed ones,[4–6] which has also been our own experience. The origin is generally attributed to the increase in the WF of ITO after such treatments,[5,16,17] which thus reduces the energy barrier for hole injection from the ITO to the polymer. The mechanism for the WF increase, however, has not been identified unambiguously.[16,17] From our observation, it clearly implies that the WF increase is related to the formation of stable oxide. This assertion is partially consistent with a recent study that connects the WF increase to the oxidation of Sn.[17] However, since In_2O_3 is dominant on the surface, the formation of stable In_2O_3 should be the major factor. Our observation also agrees with reports that demonstrate the addition of an ultrathin layer of SiO_2 on ITO increases the efficiency of molecule-based OLEDs.[18,19]

In addition to creating a boost in efficiency, a sturdy oxide layer also hinders chemical reactions at the interface between the ITO and the organic layer. As has already been described previously, samples A and B are susceptible to oxide decomposition. The metal ions generated can react with the emissive layer and reduce the device lifetime.[20,21] On the other hand, metal ions are difficult to generate if the surface oxide is stable, as on sample C. Following this point of view, a stable layer should have a similar effect. It has been confirmed that, by adding a hole transport layer between the ITO and the emissive layer, the degradation is slowed down and the stability is improved.[22] It should be mentioned, however, that the ozone treatment did not completely oxidize the ITO surface, as is evident from Fig. 1(c). The remaining conducting regions may react with the organic layer and become the possible starting regions of device failure.

V. CONCLUSIONS

In summary, we have performed a nanoscale surface electrical study of ITO films by a conducting AFM. On all the samples, a nonconducting feature is dominant on the surface and ohmic contact behavior appears on the conducting regions. With a voltage sweep of up to 8 V, reproducible field emission type tunneling is observed only on the nonconducting regions on the UV-ozone treated ITO, whereas the decomposition of oxide is observed on the other two samples. Our work suggests that the generation of stable oxide on ITO is one of the origins that leads to better device performance.

ACKNOWLEDGMENTS

The authors acknowledge Professor David Paine of Brown University for providing the Young's modulus of ITO. They also thank Shen-Shen Wang and Ju-Hung Hsu for technical assistance. This work was supported by the National Science Council of Republic of China (Grant No. 89-2215-E-007-035).

[1] J. R. Sheats, H. Antoniadis, M. Hueschen, W. Leonard, J. Miller, R. Moon, D. Roitman, and A. Stocking, Science **273**, 884 (1996).
[2] R. H. Friend *et al.*, Nature (London) **397**, 121 (1999).
[3] H. Kim, C. M. Gilmore, A. Piqué, J. S. Horwitz, H. Mattoussi, H. Murata, Z. H. Kafafi, and D. B. Chrisey, J. Appl. Phys. **86**, 6451 (1999).
[4] C. C. Wu, C. I. Wu, J. C. Sturm, and A. Kahn, Appl. Phys. Lett. **70**, 1348 (1997).
[5] J. S. Kim, M. Granström, R. H. Friend, N. Johansson, W. R. Salaneck, R. Daik, W. J. Feast, and F. Cacialli, J. Appl. Phys. **84**, 6859 (1998).
[6] S. K. So, W. K. Choi, C. H. Cheng, L. M. Leung, and C. F. Kwong, Appl. Phys. A: Mater. Sci. Process. **68**, 447 (1999).
[7] S. J. O'Shea, R. M. Atta, M. P. Murrell, and M. E. Welland, J. Vac. Sci. Technol. B **13**, 1945 (1995).
[8] M. A. Lantz, S. J. O'Shea, and M. E. Welland, Phys. Rev. B **56**, 15345 (1997).
[9] A. Bietsch, M. A. Schneider, M. E. Welland, and B. Michel, J. Vac. Sci. Technol. B **18**, 1160 (2000).
[10] From the Hertz model, we have $a^3=3Fr/4E^*$ and $1/E^*=(1-\nu_1^2)/E_1+(1-\nu_2^2)/E_2$, where a is the contact radius, F the load, r the tip radius, E the Young's modulus, and ν the Poisson ratio. With $F=60$ nN, $r=50$ nm, $E_1=81$ GPa, $\nu_1=0.42$ (for Au), and $E_2=80$ GPa, $\nu_2=0.2$ (for ITO), a is determined to be 3.7 nm.
[11] T. Nakao, T. Nakada, Y. Nakayama, K. Miyatani, Y. Kimura, Y. Saito, and C. Kaito, Thin Solid Films **370**, 155 (2000).
[12] S. M. Sze, *Physics of Semiconductor Devices* (Wiley, New York, 1981).
[13] H. Koyanagi, S. Hosaka, R. Imura, and M. Shirai, Appl. Phys. Lett. **67**, 2609 (1995).
[14] E. S. Snow, G. G. Jernigan, and P. M. Campbell, Appl. Phys. Lett. **76**, 1782 (2000).
[15] N. P. Magtoto, C. Niu, B. M. Ekstrom, S. Addepalli, and J. A. Kelber, Appl. Phys. Lett. **77**, 2228 (2000).
[16] K. Sugiyama, H. Ishii, Y. Ouchi, and K. Seki, J. Appl. Phys. **87**, 295 (2000).
[17] D. J. Milliron, I. G. Hill, C. Shen, A. Kahn, and J. Schwartz, J. Appl. Phys. **87**, 572 (2000).
[18] Z. B. Deng, X. M. Ding, S. T. Lee, and W. A. Gambling, Appl. Phys. Lett. **74**, 2227 (1999).
[19] X. M. Ding, L. M. Hung, L. F. Cheng, Z. B. Deng, X. Y. Hou, C. S. Lee, and S. T. Lee, Appl. Phys. Lett. **76**, 2704 (2000).
[20] C.-I. Chao, K.-R. Chuang, and S.-A. Chen, Appl. Phys. Lett. **69**, 2894 (1996).
[21] J. Shen, D. Wang, E. Langlois, W. A. Barrow, P. J. Green, C. W. Tang, and J. Shi, Synth. Met. **111–112**, 233 (2000).
[22] Q. T. Le, F. M. Avendano, E. W. Forsythe, L. Yan, Y. Gao, and C. W. Tang, J. Vac. Sci. Technol. A **17**, 2314 (1999).